High-frequency single-photon source with polarization control

STEFAN STRAUF[1,2]*, NICK G. STOLTZ[3], MATTHEW T. RAKHER[1], LARRY A. COLDREN[3,4], PIERRE M. PETROFF[3,4] AND DIRK BOUWMEESTER[1,5]

[1]Department of Physics, University of California, Santa Barbara, California 93106, USA
[2]Department of Physics and Engineering Physics, Stevens Institute of Technology, Hoboken, New Jersey 07030, USA
[3]Materials Department, University of California, Santa Barbara, California 93106, USA
[4]ECE Department, University of California, Santa Barbara, California 93106, USA
[5]Huygens Laboratory, Leiden University, PO Box 9504, 2300 RA Leiden, The Netherlands
*e-mail: strauf@stevens.edu

Published online: 18 November 2007; doi:10.1038/nphoton.2007.227

Optoelectronic devices that provide non-classical light states on demand have a broad range of applications in quantum information science[1], including quantum-key-distribution systems[2], quantum lithography[3] and quantum computing[4]. Single-photon sources[5,6] in particular have been demonstrated to outperform key distribution based on attenuated classical laser pulses[7]. Implementations based on individual molecules[8], nitrogen vacancy centres[9] or dopant atoms[10] are rather inefficient owing to low emission rates, rapid saturation and the lack of mature cavity technology. Promising single-photon-source designs combine high-quality microcavities[11] with quantum dots as active emitters[12]. So far, the highest measured single-photon rates are ∼200 kHz using etched micropillars[13,14]. Here, we demonstrate a quantum-dot-based single-photon source with a measured single-photon emission rate of 4.0 MHz (31 MHz into the first lens, with an extraction efficiency of 38%) due to the suppression of exciton dark states. Furthermore, our microcavity design provides mechanical stability, and voltage-controlled tuning of the emitter/mode resonance and of the polarization state.

Excitons inside semiconductor quantum dots (QDs) interact efficiently with light, making them attractive as an optically active material for single-photon sources (SPS)[5,6,12–18], LEDs (ref. 19), low-threshold lasers[20] and solar cells[21]. Under optical excitation or electrical-carrier injection, electrons and holes are created in higher energy states and subsequently relax into localized QD states. Random carrier capture leads to both geminate and non-geminate loading of the QD, causing limitations in device efficiency[22]. When a QD is loaded with a neutral exciton (X0), it can be either in a bright-state configuration with angular momentum $L_z = \pm 1$ or in a dark state with $L_z = \pm 2$. Although the bright-state configuration is dipole allowed with a typical spontaneous emission (SE) lifetime of 1 ns, the dark-state configuration is dipole forbidden and thus a long-lived state. If a QD is loaded into a dark state, a spin-flip must occur, for example involving the Fermi sea of an adjacent back gate[23], or it can be pumped through the biexciton (XX) to the bright state. Thus if a QD is triggered to emit single photons (SPs) at a high repetition rate, it occupies on average more time in dark-state configurations, which limits the maximal achievable emission rate (see Supplementary Information). Additionally, the capture of single carriers leads to submicrosecond correlation effects[14], which act in effect as dark states.

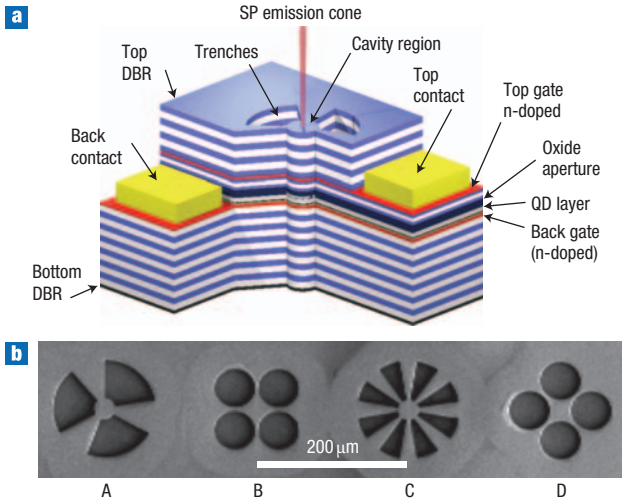

Figure 1 SPS device design. a, Schematic three-dimensional view of the SPS containing a λ-cavity region embedded between a 32-period bottom AlGaAs/GaAs DBR and a 23-period top DBR (white/blue layers). The cavity contains a single layer of InAs QDs (grey) and a mode-confining tapered AlO_x region (dark blue). Selective countersink etching allows separate global contacting (yellow) of the n-doped top and bottom gate layers (red). **b**, Scanning electron micrograph of various geometries of the trench design (top view). The inner lateral cavity area has a diameter of ∼20 μm. The remaining small bars provide lateral electrical contacts.

To eliminate dark-state configurations we aimed to load a QD embedded in a microcavity with a single electron. Subsequent electron–hole pair capturing owing to optical (or electrical) excitation would create predominantly charged excitons (X−) in a singlet configuration. In such a case, recombination is always expected to be bright and an SPS can continuously fire SPs with

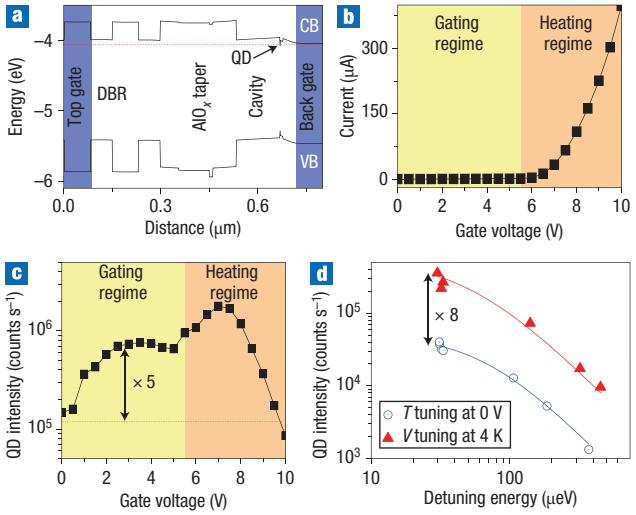

Figure 2 Influence of gate voltage on SPS performance. a, Schematic energy band diagram. The tunnel barrier width between the back gate and the QD is 25 nm. CB, conduction band; VB, valence band. **b**, Current–voltage characteristic of the entire SPS array recorded at 4 K. **c**, Single QD intensity as a function of gate voltage for a type B (from Fig. 1b) device under 780 nm excitation. **d**, Comparison of SPS intensity as a function of QD/mode detuning energy using the cryostat heater at zero gate voltage (*T* tuning, blue circles) and for fixed cryostat temperature (4 K) and gate voltages between 5 and 9 V (*V* tuning, red triangles). Detuning energies are taken from lorentzian line-shape analysis.

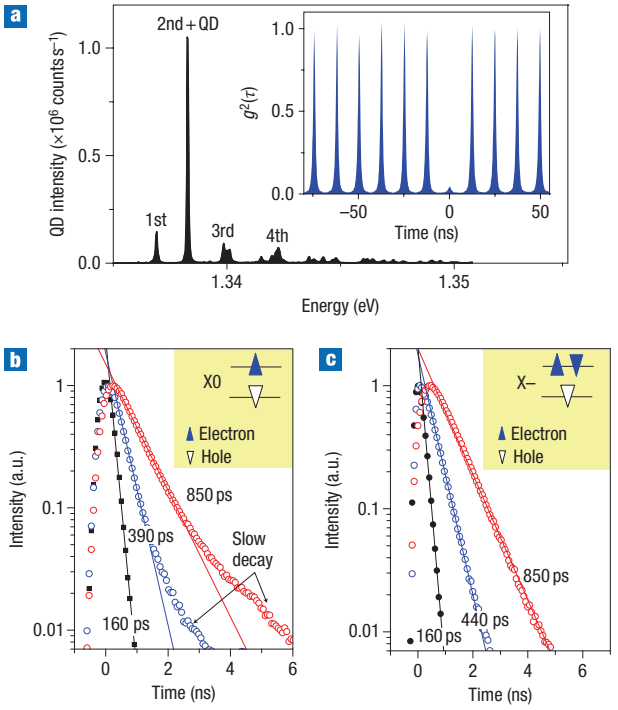

Figure 3 Single QD characterizations. a, Cavity mode spectrum with a neutral QD coupled to a second-order mode at 7.3 V bias. Inset: Second-order correlation function $g^2(\tau)$ recorded with 10 nW pump power. Note that submicrosecond correlation effects[14] are absent under biased conditions for both QD charge states even at lowest pump powers. **b**, Lifetime measurements for QD loaded with X0 under off-resonance (red circles) and on-resonance (blue circles) conditions. Black data points indicate scattered laser light corresponding to 160-ps system resolution. **c**, Comparable lifetime measurements for a QD loaded with X−. Note the mono-exponential decay in contrast to the bi-exponential decay of X0.

rates approaching the SE lifetime limit. Additional electrons can either be injected through electrical gates or provided by doping QDs or their surroundings or both.

Although controlled loading of single QDs has been demonstrated[23,24], implementation of electrical gates into high-*Q* cavities has not yet been achieved. To this end we have developed oxide-tapered high-*Q* microcavities based on a rugged trench design. Figure 1a shows a device schematic. A layer of QDs inside a wavelength-lang cavity (λ-cavity) is sandwiched between two distributed Bragg reflectors (DBR). A top electrical gate and a tunnel back gate with 25-nm barrier are formed adjacent to the QDs (see Methods for details). These n-doped layers provide an embedded electrical gating structure to control the QD loading process and local current heating within the cavity. Air-etched GaAs micropillars are typically fabricated with submicrometre diameters to confine the mode volume[11,13]. To avoid difficulties associated with micrometre-scale electrical contacts, we use trenches with various geometries etched down into the bottom DBR (Fig. 1b). These trenches are used to define an AlO_x oxidation front, providing high-quality factors up to 50,000 and simultaneously optical-mode confinement[15]. This design provides good mechanical stability, the possibility of controlling the mode degeneracy, and it allows global contacting by countersink etching two contacts to an entire SPS array.

Figure 2a shows a schematic of the band structure including top and back gates (blue areas). The bottom gate is grounded and voltage is applied to the top gate. Optical emission is probed under non-resonant laser excitation into the GaAs. At negative bias voltages below −2 V the QD emission completely quenches, in analogy to gated structures without a cavity[24]. For voltages above about 5.5 V, carriers overspill and create a current breakthrough, as shown in the current–voltage (*I*–*V*) curve in Fig. 2b. This creates two useful regimes for SPS operation. For voltages below breakthrough, one can manipulate the QD loading process as shown in the following. Above breakthrough, the electrical current causes localized heating (on-chip heater), which can be used to fine-tune the QD/mode resonance (Fig. 2c,d).

Interestingly, a strong fivefold increase in QD emission is observed for voltages of 2–5 V (Fig. 2c). In this regime, no spectral shift of the QD exciton occurs. This excludes both QD charging (X– formation) and spectral QD/mode detuning (Purcell effect[6]) as an explanation. Controlled QD/mode tuning can either be achieved at zero gate voltage using the cryostat heater (method A) or at a fixed base temperature (4 K) and increasing the gate voltage above 5 V (method B), as shown in Fig. 2d. For method A, the QD transition has a 40-fold intensity enhancement if tuned into resonance (blue circles). Method B creates an additional eightfold enhancement for all detuning conditions (red triangles). Simultaneously, the X0 transition displays a Purcell factor of two (see Fig. 3b), independent of the tuning method. Thus the intensity enhancement is independent of the actual SE rate, suggesting a relation to the QD loading process[25]. These findings suggest that the voltage-induced enhancement (Fig. 2c,d) is related to field-enhanced carrier capture processes. Indeed, if single QDs are optically pumped into SE saturation, the voltage-induced intensity enhancement also saturates (not shown). However, practically, SPSs are not operated at saturation because of degraded SP purity. Therefore,

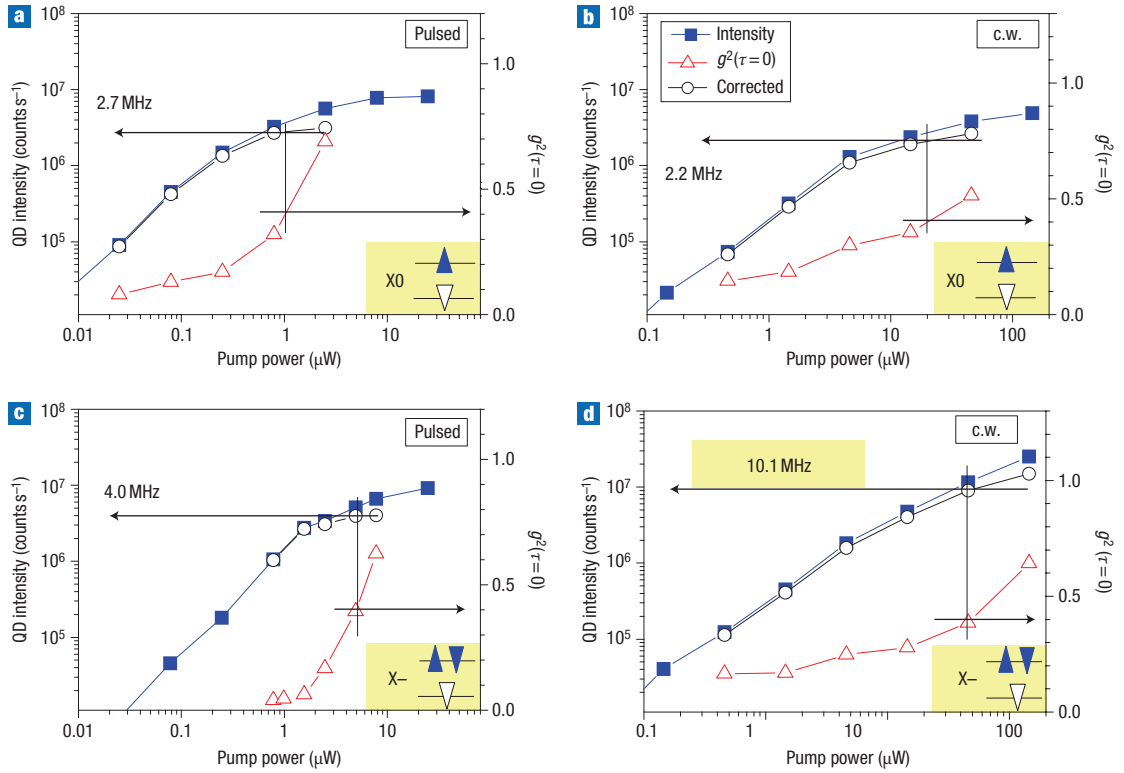

Figure 4 Impact of QD charging on SPS performance. a–d, QD intensity (blue squares, left *y* axis) and corresponding $g^2(\tau = 0)$ values from coincidence measurements (open red triangles, right *y* axis). Intensity data are corrected for background emission (open black dots; see Methods). Two devices are compared: one with X0 (**a**, **b**) and one with X– on resonance (**c**, **d**). For each charging state we compare pulsed laser excitation at 780 nm (**a**, **c**) and c.w. laser excitation at 630 nm (**b**, **d**). Arrows indicate SP intensities at $g^2(\tau = 0) = 0.4$, close to QD saturation. Note the noticeably improved count rates for charged QDs under c.w. excitation.

the achieved voltage-controlled enhancement is of high practical importance as it allows higher SP rates at a comparable injection level while minimizing background contributions that otherwise compromise the SP purity.

Single-photon sources are characterized by strong photon antibunching signatures[5,6]. Figure 3a shows a spectrum of a single QD loaded with X– and tuned in resonance with a degenerate cavity mode. The inset shows the corresponding second-order correlation function, $g^2(\tau)$, displaying a zero delay time peak area of 4%. This corresponds to a 25-fold decrease in unwanted multiphoton emission events compared with attenuated coherent light sources. Devices typically display a 40-fold enhanced SP emission rate if sharp exciton lines are tuned into spectral resonance (Fig. 2d). These results were achieved for QDs with an SE lifetime of about 1 ns, similar to QDs in bulk GaAs. They are thus spectrally, but not spatially, on resonance. In such a case intensity enhancement is entirely caused by enhanced geometrical collection efficiency and not related to the Purcell effect. In about a third of devices, the QDs under consideration are spatially on resonance and display a Purcell factor of from two to four if tuned spectrally into resonance. To separate effects related to random positioning of QDs from effects caused by charging and applied voltages, we concentrate on devices with a Purcell factor of approximately two (Fig. 3b,c).

To show that X– is better suited for an SPS than X0, we first have to identify the X0 and X– transitions of individual QDs. In high-*Q* cavities, clear identification based on spectral signatures, that is, the typical 5–6 meV Coulomb charging separation[24], is rather difficult because spectra are largely altered by the underlying mode distribution and stop band. However, as has been demonstrated[23], time-resolved measurements of QDs in gated structures display a mono-exponential decay for the X– transition and a pronounced bi-exponential decay for X0. Figure 3b,c shows lifetime measurements for single QDs located in two different devices, clearly distinguishing between bi-exponential (Fig. 3b) and mono-exponential (Fig. 3c) decay for both off-resonance (red circles) and on-resonance (blue circles) conditions with a degenerate mode, supporting our assignment of X0 and X–.

We investigated the SPS device performance by recording both intensity and antibunching signatures as a function of pump power (Fig. 4a–d). With increasing pump power, antibunching signatures bleach out owing to QD saturation and SE coupling from other QDs at higher pump powers[20], limiting the maximal achievable SP rates. To compare devices pumped under pulsed and continuous-wave (c.w.) excitation conditions we chose a working point close to QD saturation, where $g^2(\tau = 0) = 0.4$, that is, when the SPS still performs 2.5 times better than an attenuated laser source. Before comparison, the measured intensity data had been corrected for the multiphoton background to extract the bare SP rate (see Methods). Two devices with degenerate modes were chosen for comparison, one with X0 on resonance (Fig. 4a,b) and one with X– on resonance (Fig. 4c,d). Under pulsed excitation, measured SP rates are 2.7 MHz for the X0 and 4.0 MHz for the X– transition, respectively. If corrected for the 13% detection efficiency, these devices emit into the first lens

with a record high SP rate of 21 MHz for X0 and 31 MHz for X−. From these data and the given repetition rate (82 MHz) one can estimate an SP extraction efficiency η of 26% for X0 and 38% for X−. If a higher purity of SP is required[26], one can, for example, operate the X− devices at 1 μW pump power (Fig. 4c) leading to $g^2(0) = 0.05$, an SP rate of 21 MHz and $\eta = 25\%$.

If one drives the two-level system even faster than with an 82 MHz repetition rate, one would expect even higher SP rates of about 870 MHz up to the SE lifetime limit (This limit is estimated using the measured (Purcell enhanced) exciton lifetime of 440 ps (2.3 GHz) modified by the cavity-mode collection efficiency of 38%.) Pumping the single QD under c.w. excitation thus probes for the ultimate limit. We performed the same SPS characterization under c.w. excitation at 632 nm (Fig. 4b,d). Surprisingly, for QDs loaded with X0, maximal achievable SP rates saturate at about 2.2 MHz, which is comparable to the pulsed excitation experiment (Fig. 4b). This demonstrates that the emission rate of X0 is severely limited by dark states. Most strikingly, c.w. excitation of an SPS with X− on resonance yields an SP rate of 10.1 MHz (Fig. 4c), corresponding to 78 MHz if corrected for detection efficiency, which is a threefold improvement over the X0 case (see Methods). In contrast to the case of X0, the SP rate for X− saturates slowly and one can estimate 116 MHz at the highest pump powers near 150 μW. At lower pump powers the X−/X0 ratio is close to unity. These findings are in quantitative agreement with a rate-equation model (see Supplementary Information). At low pump rates there is enough time for a spin-flip to occur between excitation events, and X0 dark states can become bright again, leading to a ratio of unity. At higher pump rates the XX creates a path back into the bright state for X0. In a cavity the XX is inhibited if X is on resonance, which limits the X0 recovery time out of dark states compared with the Purcell enhanced recombination rate of the X− transition, which is always bright. Although these c.w. experiments clearly demonstrate that a threefold improvement can be achieved by using X−, the nature of c.w. excitation does not in principle allow for on-demand operation. Thus the highest achieved count rate for on-demand operation of our SPS devices is 31 MHz ($\eta = 38\%$), constituting a fivefold improvement compared with other SPSs (refs 5–18; see Methods), which makes them very attractive for quantum light applications.

In addition to high SP rates, a practical device for quantum communication can provide on-chip selection of the emitted polarization state. Non-degenerate cavity modes allow the generation of an SPS emitting either horizontal (H) or vertical (V) polarized SPs, as shown earlier[27,28]. To actively switch between polarization states on the chip, one must tune the QD emission either to the energy of the H- or V-polarized mode. To this end, we explored several types of trenches (Fig. 1b). Mode separation increases with decreasing aperture opening and/or longer oxidation time[15]. Depending on trench geometry and oxidization times, the cavity modes are either degenerate (type B, Fig. 5a) or non-degenerate (type D, Fig. 5b), with splitting energies of about 300 μeV and a contrast ratio of 57:1 between H- and V-polarized modes. For comparison to the results of Figs 2–4, we chose a type D device containing X0. Method A (cryostat heater) was used to achieve QD/mode resonance (Fig. 5c). Coupling of a single QD to either the H or V mode is manifested by a Purcell factor of 2.7, which is comparable to the type B devices. The measured intensity enhancement is about twofold lower compared with the type B devices, as expected if only one QD polarization state is coupled out using a non-degenerate mode. The ability to control the polarization state on the chip will thus reduce the overall SPS device efficiencies by a factor of two. The switching speed using temperature is

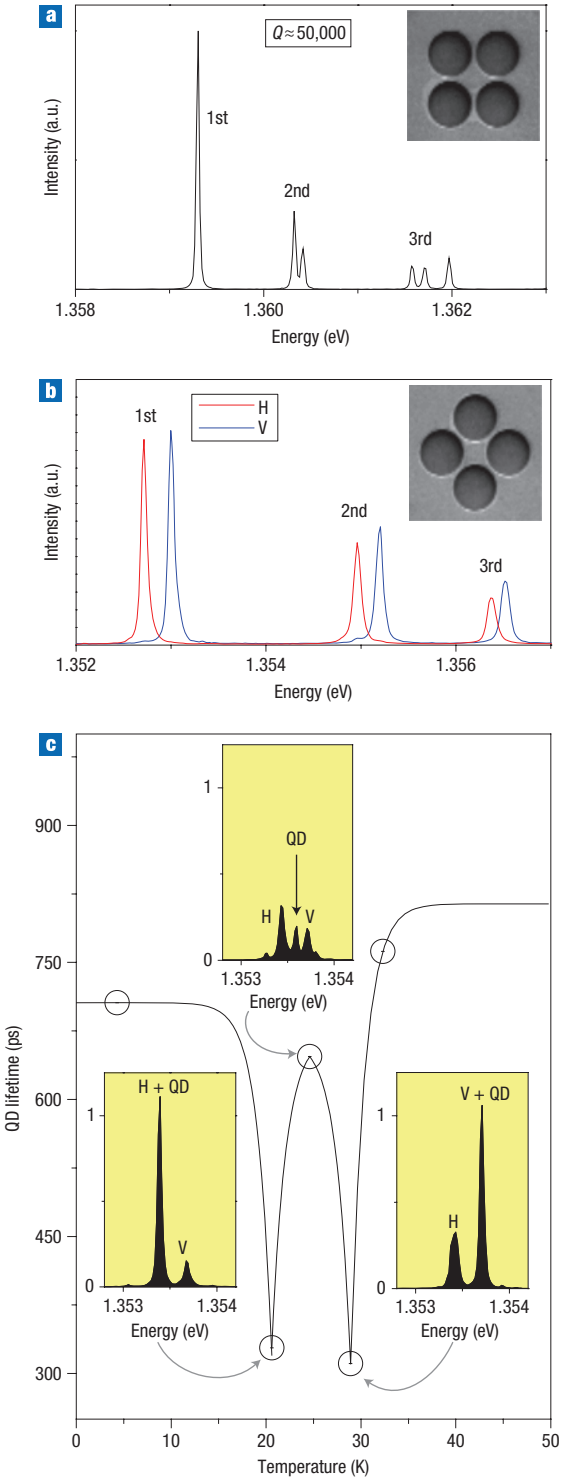

Figure 5 Demonstration of polarization control. a, Cavity mode spectrum for a type B device (depicted in the inset) showing polarization-degenerate modes (*Q* factors up to 50,000). **b**, Polarization-resolved spectra of a type D device (depicted in the inset) showing linear polarization splitting of 270 μeV for the first-order cavity mode (1st). H indicates horizontal polarization and V vertical polarization. **c**, Temperature tuning of a single QD exciton transition through the non-degenerate cavity modes. Coupling to either of the H- or V-modes is manifested by an enhanced lifetime from about 800 ps off resonance to 300 ps on resonance (*y* axis). Insets show spectra taken for different QD/mode detuning conditions.

nevertheless very limited. To overcome these limitations Stark-shift tuning[29] in an applied electrical field can be used. Our rugged cavity trench design offers possibilities to integrate additional lateral gates; this will be the subject of another study.

Ultrahigh SP rates are a combination of several effects. First, large geometrical extraction efficiency is provided by the cavity design. Second, the observed single QD Purcell effect contributes a factor of from two to four. Third, the positive bias voltage creates a fivefold intensity enhancement at comparable optical injection levels, reducing background contributions that otherwise compromise SP purity. Finally, QDs loaded with X– effectively reduce dark states, which further increase the SPS efficiency by a factor of three. Together, these effects contribute to the observed record high rates of SPs on demand up to 31 MHz, and promise rates above 116 MHz as investigated by the c.w. experiments. Nevertheless, devices still do not approach the SE lifetime limit of about 870 MHz (ref. 27). One reason for this is that non-geminate-carrier capture allows for a single-hole capture directly after the X– state has decayed into the single electron state. This leads to formation of X0 rather than X–, and dark-state configurations are again possible.

In conclusion, we fabricated an SPS by integrating high-Q (50,000) GaAs/AlGaAs microcavities with embedded oxide-tapered apertures, a rugged trench design, as well as buried electrical gates allowing controlled loading and Purcell tuning of individual InAs QDs. We observed single photons at record high rates up to 31 MHz, and SP extraction efficiencies up to 38% if negatively charged excitons were used. Additionally, we demonstrated tunability of the spectral mode degeneracy and also controlled coupling of single QDs to either H- or V-polarized cavity modes. This type of SPS is of direct interest for applications in quantum information science.

METHODS

SAMPLE PREPARATION

Devices are grown by molecular beam epitaxy on a semi-insulating GaAs (100) substrate with a 0.1-μm buffer layer. There are four sections in the structure, the bottom mirror, the active region, the oxide-aperture region and the top mirror as described in more detail in our previous study[15]. The optical GaAs cavity is Si n-doped up to 25 nm below the single layer of InAs QDs, providing a tunnel back gate. The fifth GaAs DBR period above the aperture region is Si n-doped, providing a top gate. Two etch windows with selective countersink depth are created using reactive-ion etching in Cl_2 plasma away from the SPS devices and contacted using a Ti/Pt/Au metallization. Cavity trenches were formed by optical lithography and reactive-ion etching to penetrate approximately five mirror periods into the bottom DBR. This etches small trenches in the surface that are used to define the AlO_x oxidation front. Tapered AlO_x apertures are formed laterally during steam oxidation within the cavity area, creating inner openings of 0.5–2 μm, effectively confining the mode volume[15].

OPTICAL CHARACTERIZATION

Micro-photoluminescence (micro-PL) measurements were performed using a microscope objective with numerical aperture NA = 0.4. Photon coincidences were recorded as a histogram of start–stop events and provide a measure of the second-order correlation function $g^2(\tau) = \langle I(t)I(t+\tau)\rangle / \langle I(t)\rangle\langle I(t)\rangle$, where $\langle I(t)\rangle$ is the expectation value of the photon intensity at time t. Additional details can be found in refs 15 and 20. Time-resolved single QD measurements have been performed under pulsed TiSa-laser excitation (150 fs pulsewidth) at a repetition rate of 82 MHz. The single QD PL signal was spectrally filtered with a 1-nm bandpass and coupled into a single-photon detector with about 130 ps timing jitter.

DATA ANALYSIS

Measured SP count rates were corrected for multiphoton emission events by multiplying by $(1 - g^2(\tau = 0))^{0.5}$ as introduced in ref. 13. A detection efficiency of 13% was estimated by measuring losses of all optical components at 920 nm and by using the detector efficiency. The total amount of single photons emitted into the first lens is 7.7 times the value shown on the y axis in Fig. 4. Aperture losses at the first lens can be neglected because our high-Q cavity emits into a far-field angle of only 10°, in contrast with earlier work[13,14] with low-Q cavities where 78% of the light was lost at the first lens. With these corrections, our highest SP rate with on-demand character is 31 MHz. Highest measured SP rates of 200 kHz were reported in ref. 14 under resonant excitation. For comparison with our experiments the off-resonance value of 50 kHz should be used, but no detection efficiency was given in ref. 14. We have thus used the stated SPS collection efficiency from ref. 14 of 8% multiplied by the repetition rate, yielding 6 MHz. From this number we estimate a fivefold improvement compared with former works.

X–/X0 ENHANCEMENT FACTOR

The bare X–/X0 ratio from the c.w. experiments is 4.6 (10.1 MHz/2.2 MHz). Because it is difficult to control the charging state and simultaneously also the QD/mode resonance within the same device, we compared two very similar devices, one loaded with X0 and tuned into resonance and one with X–. Thus, it is necessary to correct for the difference between the devices, which can be taken from the pulsed experiments close to saturation (4.0 MHz/2.7 MHz), leading to a corrected improvement factor of 3.1. (See Supplementary Information for a theoretical foundation in a rate-equation analysis.)

Received 7 June 2007; accepted 16 October 2007;
published 18 November 2007.

References

1. Bouwmeester, D., Ekert, A. K. & Zeilinger A. *The Physics of Quantum Information* (Springer, Berlin, 2000).
2. Gisin, N., Ribordy, G., Tittel, W. & Zbinden, H. Quantum cryptography. *Rev. Mod. Phys.* **74,** 145–195 (2002).
3. Boto, A. N. *et al.* Quantum interferometric optical lithography: exploiting entanglement to beat the diffraction limit. *Phys. Rev. Lett.* **85,** 2733–2736 (2000).
4. Knill, E., Laflamme, R. & Milburn, G. J. A scheme for efficient quantum computation with linear optics. *Nature* **409,** 46–52 (2001).
5. Lounis, B. & Orrit, M. Single-photon sources. *Rep. Prog. Phys.* **68,** 1129–1179 (2005).
6. Shields, A. J. Semiconductor quantum light sources. *Nature Photon.* **1,** 215–223 (2007).
7. Waks, E. *et al.* Quantum cryptography with a photon turnstile. *Nature* **420,** 762 (2002).
8. Lee, T.-H. *et al.* Oriented semiconducting polymer nanostructures as on-demand room-temperature single-photon source. *Appl. Phys. Lett.* **85,** 100–102 (2004).
9. Kurtsiefer, C., Mayer, S., Zarda, P. & Weinfurter, H. Stable solid-state source of single photons. *Phys. Rev. Lett.* **85,** 290–293 (2000).
10. Strauf, S. *et al.* Quantum optical studies on individual acceptor bound excitons in a semiconductor. *Phys. Rev. Lett.* **89,** 177403 (2002).
11. Vahala, K. Optical microcavities. *Nature* **424,** 839–846 (2003).
12. Michler, P. *et al.* A quantum dot single-photon turnstile device. *Science* **290,** 2282–2285 (2000).
13. Pelton, M. *et al.* Efficient source of single photons: A single quantum dot in a micropost microcavity. *Phys. Rev. Lett.* **89,** 233602 (2002).
14. Santori, C. *et al.* Submicrosecond correlations in photoluminescence from InAs quantum dots. *Phys. Rev. B* **69,** 205324 (2004).
15. Stoltz, N. G. *et al.* High-quality factor optical microcavity using oxide apertured micropillars. *Appl. Phys. Lett.* **87,** 031105 (2005).
16. Yuan, Z. *et al.* Electrically driven single-photon source. *Science* **295,** 102–105 (2002).
17. Chang, W.-H. *et al.* Efficient single-photon sources based on low-density quantum dots in photonic-crystal nanocavities. *Phys. Rev. Lett.* **96,** 117401 (2006).
18. Takemoto, K. *et al.* An optical horn structure for single-photon source using quantum dots at telecommunication wavelength *J. Appl. Phys.* **101,** 081720 (2007).
19. Colvin, V., Schlamp, M. & Alivisatos, A. P. Light-emitting diodes made from cadmium selenide nanocrystals and semiconducting polymer. *Nature* **370,** 354–357 (1994).
20. Strauf, S. *et al.* Self-tuned quantum dot gain in photonic crystal lasers. *Phys. Rev. Lett.* **96,** 127404 (2006).
21. Gur, I., Fromer, M. A., Geier, M. L. & Alivisatos, A. P. Air-stable all inorganic nanocrystal solar cell processed from solution. *Science* **310,** 462–465 (2005).
22. Urayama, J., Norris, T. B., Singh, J. & Bhattacharya, P. Observation of phonon bottleneck in quantum dot electronic relaxation. *Phys. Rev. Lett.* **86,** 4930–4933 (2001).
23. Smith, J. M. *et al.* Voltage control of the spin dynamics of an exciton in a semiconductor quantum dot. *Phys. Rev. Lett.* **94,** 197402 (2005).
24. Warburton, R. *et al.* Optical emission from a charge-tunable quantum ring. *Nature* **405,** 926–929 (2000).
25. Holtz, P. O. *et al.* Enhanced luminescence from InAs/GaAs quantum dots. *Proc. SPIE* **6401,** 64010I (2006).
26. Waks, E., Santori, C. & Yamamoto, Y. Security aspect of quantum key distribution with sub-Poissonian light. *Phys. Rev. A* **66,** 042315 (2002).
27. Moreau, E. *et al.* Single-mode solid-state single photon source based on isolated quantum dots in pillar microcavities. *Appl. Phys. Lett.* **79,** 2865–2867 (2001).
28. Unitt, D. C., Bennett, A. J., Atkinson, P., Ritchie, D. A. & Shields, A. J. Polarization control of quantum dot single-photon sources by means of dipole-dependent Purcell effect. *Phys. Rev. B* **72,** 033318 (2006).
29. Zrenner, A. *et al.* Coherent properties of a two-level system based on a quantum-dot photodiode. *Nature* **418,** 612–614 (2002).

Acknowledgements

We would like to thank D. Cohen for fruitful discussions. This work was supported through DARPA, NSF and ARO grants.
Correspondence and requests for materials should be addressed to S.S.
Supplementary Information accompanies this paper on www.nature.com/naturephotonics.